JOURNAL OF MATERIALS SCIENCE 29 (1994) 6295–6300

Solubility of CaO in $CaTiO_3$

M. ČEH, D. KOLAR
J. Stefan Institute, University of Ljubljana, Jamova 39, 61000 Ljubljana, Slovenia

The solubility and mode of incorporation of CaO in $CaTiO_3$ were studied by X-ray powder diffraction, scanning and transmission electron microscopy, electron probe microanalysis and equilibrium electrical conductivity measurements. The presence of $Ca_4Ti_3O_{10}$ in samples containing > 0.3 mol% excess CaO was confirmed by direct microscopic examination. Measurements of the equilibrium electrical conductivity showed no detectable shift in the conductivity profile for CaO–excess $CaTiO_3$, thus setting an upper limit of 100 p.p.m. for the solubility of CaO in $CaTiO_3$. The excess CaO is incorporated into $CaTiO_3$ by formation of Ruddlesden–Popper type planar faults, which are layers of CaO coherently intergrown with $CaTiO_3$. Ordering of these planar faults leads to the formation of the stable compound $Ca_4Ti_3O_{10}$.

1. Introduction

Until now, relatively little has been known about the solubility or mode of incorporation of excess CaO in $CaTiO_3$. Despite many investigations of phase equilibria in the CaO–TiO_2 system and of the defect structure of CaO–excess $CaTiO_3$, the exact solubility limit of CaO in $CaTiO_3$ has not yet been determined. Early studies of phase relations in the CaO–TiO_2 system [1–3] showed very similar parts of the phase diagram between $CaTiO_3$ and TiO_2. However, a disagreement existed about the number of possible compounds and their stability in the region from $CaTiO_3$ to CaO. Later studies of phase relations [4] showed the existence of a CaO rich compound, $Ca_3Ti_2O_7$. It was also suggested that there is a phase width for $CaTiO_3$ on the CaO rich side, up to about 2–3 mol % excess CaO at 1200 °C. Roth [5] reported that $Ca_3Ti_2O_7$ is not the only stable compound in the system between $CaTiO_3$ and CaO; $Ca_4Ti_3O_{10}$ also exists as a stable phase. Both $Ca_4Ti_3O_{10}$ and $Ca_3Ti_2O_7$, have a pseudotetragonal unit cell. The dimensions of the unit cells indicate that $Ca_3Ti_2O_7$ has double perovskite layers interleaved with a CaO layer, while $Ca_4Ti_3O_{10}$ has triple perovskite layers interleaved with the CaO layer. Kwestroo and Papping [6] found that the compound $Ca_3Ti_2O_7$ is formed only above 1480 °C, thus confirming the results of Cocco [7]. The most recent phase diagram of the CaO–TiO_2 system [8] is in good agreement with the phase diagram presented by Roth [5]. Even though this phase diagram shows no solubility for CaO in $CaTiO_3$ over the temperature range 1400–1600 °C, the precise solubility limit for CaO in $CaTiO_3$ and its mode of incorporation still needs to be determined.

Possible point defect incorporation reactions for the accommodation of excess CaO in the $CaTiO_3$ lattice in the single phase system are as follows

$$CaO \rightarrow Ca_{Ca}^{x} + V_{Ti}^{''''} + O_O^x + 2V_O^{\cdot\cdot} \quad (1)$$

$$CaO \rightarrow Ca_i^{\cdot\cdot} + O_i'' \quad (2)$$

$$2CaO \rightarrow Ca_{Ca}^{x} + Ca_{Ti}'' + 2O_O^x + V_O^{\cdot\cdot} \quad (3)$$

where ^{x} is neutral, $''$ negative and $\cdot\cdot$ is positive.

The defect notation is that proposed by Kröger and Vink [9]. The formation of interstitial $Ca_i^{\cdot\cdot}$ and O_i'', Equation 2, is considered unlikely to be due to the close packed structure of the perovskite. This has been substantiated by the high values calculated by Lewis and Catlow [10] for the Frenkel energies compared with the Schottky energies in structural analogue $BaTiO_3$, as well as by conductivity, thermogravimetric and diffusion measurements [11, 12]. The substitution of Ca on Ti sites, Equation 3, must also be considered, since it has been determined that Ca^{+2} ions can occupy titanium sites in $BaTiO_3$ [13, 14].

An alternative mechanism for accommodating the excess CaO in $CaTiO_3$ is by structural modification of the type described by Ruddlesden and Popper for the case of SrO–excess $SrTiO_3$ [15, 16]. In $SrTiO_3$, a large excess of SrO can be accommodated by insertion of individual layers of SrO between blocks of the perovskite structure. These ordered structures correspond to a homologous series of compounds, $SrO.nSrTiO_3$, where n corresponds to the number of perovskite layers between the SrO layers [17]. Such structures have been directly observed by Tilley [18] using transmission electron microscopy. Similar structures were observed by Fujimoto *et al.* [19] who studied the microstructure of non-stoichiometric $(Sr_{0.85}Ca_{0.15}O)_{1.02}TiO_2$ compositions. The ALCHEMI technique was used to determine the site occupancy of Ca atoms in Ti sites in this A-site excess perovskite. However, the results showed that no Ca atoms occupy Ti sites and that point defects such as Ca_{Ti}'' are not formed. Instead, it was found that the (Sr, Ca)O–excess formed insertion planar faults of NaCl type.

Most studies of the defect structure of CaO–excess $CaTiO_3$ are based on measurements of equilibrium

0022–2461

electrical conductivity as a function of oxygen partial pressure and temperature. Balachandran and Eror [20] reported that the electrical conductivity measurements of CaO–excess $CaTiO_3$ (Ca/Ti > 1) were found to be similar to those obtained on samples with the ideal calcium to titanium ratio of Ca/Ti = 1.00 [21]. No shift in the conductivity minimum was observed for CaO–excess samples compared to stoichiometric $CaTiO_3$. They suggested that the incorporation of the excess CaO in $CaTiO_3$ does not generate charged point defect species, and that the excess CaO is accommodated by the formation of a shear structure, as in the case of $SrTiO_3$ [16]. In contrast, Han *et al.* [22], who employed the same liquid mix technique to prepare their non-stoichiometric samples, noticed a slight shift in the electronic *n*-type to *p*-type transition to a lower value of $P_{O_2}^{o}$ in their conductivity measurements. They concluded that there is substitution of Ca on Ti sites with compensating oxygen vacancies, $V_O^{\cdot\cdot}$, drawing upon the behaviour of its structural analogue, $BaTiO_3$ [23, 24]. This apparent discrepancy was to some extent clarified by Udayakumar and Cormack [25] who employed the atomistic computer simulation techniques to study the mode of incorporation of excess alkaline earth oxides, AO (A = Ba, Sr, Ca), into the alkaline earth titanates, $ATiO_3$. The computed energy of 10.11 eV, which is needed for the formation of $V_{Ti}^{''''}$, titanium vacancies, and $V_O^{\cdot\cdot}$, oxygen vacancies, according to Equation 1, makes this reaction energetically unfavourable and not likely to occur. A similar result was obtained when the energy for the substitution of Ca on Ti sites, according to Equation 3, was calculated. A high solution energy of 4.8 eV prohibits solubility of CaO in $CaTiO_3$. In order to examine the possibility of CaO excess incorporation through formation of shear structures, Udaykumar and Cormack calculated the formation energies of the compounds $Ca_3Ti_2O_7$ and $Ca_4Ti_3O_{10}$ according to the following equation

$$CaO + nCaTiO_3 \rightarrow CaO \cdot nCaTiO_3 \quad (n = 2, 3) \tag{4}$$

and obtained values of 0.19 and 0.18 eV, respectively. The relatively low energies of formation of these compounds seem to signify the energetic feasibility of the incorporation of shear structures of Ruddlesden–Popper layers, but no direct experimental evidence was given.

The purpose of the present study was to apply a wide range of analytical techniques including X-ray diffraction, scanning and transmission electron microscopy, electron probe microanalysis and equilibrium electrical conductivity measurements in order to clarify the solubility of and the mode of CaO incorporation in $CaTiO_3$.

2. Experimental procedure

$CaTiO_3$ powders were synthesized from high purity $CaCO_3$ (Merck, p.a.) and TiO_2 (Fluka AG, p.a.) by solid state reaction. Samples with the following Ca/Ti ratios were prepared: 1.000, 1.003, 1.005, 1.01, 1.02, 1.05 and 1.1 which correspond to 50.000, 50.075, 50.125, 50.25, 50.50, 51.22 and 52.34 mol % CaO. The starting mixtures of carefully weighed $CaCO_3$ and TiO_2 powders were wet milled and pressed into pellets. Specimens were then calcined three times at 1200 °C for 24 h. Calcined powders were wet milled in a zirconia mill for 1 h. Powders with different Ca/Ti ratios were pressed into pellets at 150 MPa and sintered at 1350, 1450 and 1550 °C from 4 to 36 h.

Polished sections for microscopic examination were prepared by diamond polishing in a medium of absolute ethanol. Water was determined to be an inappropriate medium for CaO-rich $CaTiO_3$. Grain structures were revealed after thermal etching at 1450 °C for 15 min. Polished surfaces were examined by optical and scanning electron microscopy (SEM) using a Jeol JXA 840-A electron microscope. The composition of phases was determined by wavelength-dispersive X-ray microanalysis (WDS) using a Jeol JXA 840-A equipped with a Tracor WDS analytical system.

Thin foil specimens for transmission electron microscopy (TEM) were prepared by ion-beam milling at 3.8 kV and examined in a transmission electron microscope Jeol JEM 2000-FX equipped with Link energy-dispersive X-ray analyser (EDS).

Ground samples were prepared for X-ray powder diffraction (XRD) studies. X-ray diffraction patterns of samples were recorded on a Philips PW 1710 powder diffractometer operating at 45 kV, 30 mA and $1^\circ\ min^{-1}$ scan rate with CuK_α radiation.

The conductivity was measured by the four-point d.c. technique, using both polarities of applied currents by a constant current source in the range 10^{-4} to 10^{-1} A to maintain a voltage drop of approximately 0.5 V which was measured by an HP 3456 A digital voltmeter. All conductivity measurements were made at 800 °C. The oxygen partial pressures surrounding the samples were obtained by mixtures of Ar/O_2. The resulting oxygen activity was determined by measurement of the e.m.f. from a CaO-stabilized ZrO_2 cell, which was located adjacent to the samples. Special care was given to the preparation of the samples for the conductivity measurements. $CaTiO_3$ powders with different Ca/Ti ratios were pressed into rectangular bars (12 × 3 × 4 mm) at 150 MPa, and were fired at 1000 °C for 1 h. All faces and edges were cleaned to remove contamination from the steel die. Four holes were then drilled into each rectangular bar

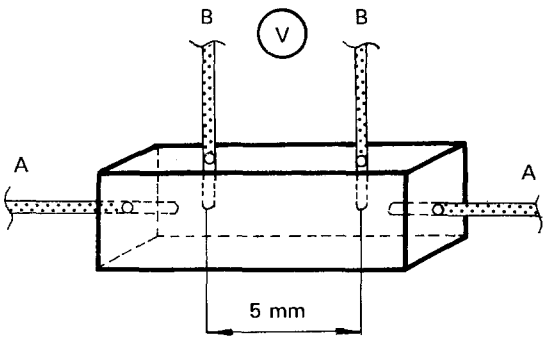

Figure 1 A schematic illustration of a sample used in the equilibrium electrical conductivity measurements: (A) current leads, (B) voltage leads.

and 2 cm lengths of 0.3 mm platinum wire were inserted into each hole (Fig. 1). Two platinum wires (marked A) were used as current leads and the other platinum wires (marked B) served to measure the voltage drop across the sample. The bars were then sintered at 1500 °C for 1 h in air. During the densification process a firm contact was formed between the inserted platinum wires and the material. The grain size ranged from 20 to 30 μm and the densities were > 95% of the theoretical value.

3. Results and discussion

Specimens having Ca/Ti ratios of 1.00, 1.02 and 1.05 were examined by X-ray diffraction (XRD). For samples that were sintered at 1350 °C, X-ray diffractograms were identical for all the compositions and showed only the presence of $CaTiO_3$. No other phases, i.e. CaO or possibly $Ca(OH)_2$, were detected, thus indicating the complete solubility of CaO in $CaTiO_3$. However, no change in lattice parameters of $CaTiO_3$ was observed for the sample with a Ca/Ti ratio of 1.05, that would support the formation of solid solution by one of the reactions in Equations 1–3. After sintering the samples with Ca/Ti > 1 at 1550 °C, a calcium-rich second phase, identified as $Ca_4Ti_3O_{10}$, was detected in the composition, having a Ca/Ti ratio of 1.05. Since most of the diffraction peaks of $CaTiO_3$ and $Ca_4Ti_3O_{10}$ overlap at higher 2θ angles, only the portion of the X-ray diffractogram up to 30° 2θ is presented, where the differences in diffraction patterns between $CaTiO_3$ and $Ca_4Ti_3O_{10}$ are easy to distinguish (Fig. 2).

Scanning electron microscopy (SEM) of sintered samples with Ca/Ti > 1 supported the results of XRD. In samples sintered at 1350 °C, no additional phases were detected within $CaTiO_3$ grains or at the grain boundaries. In samples sintered at 1550 °C, however, thermal etching revealed the presence of a secondary phase in the shape of lamellae (Fig. 3). According to

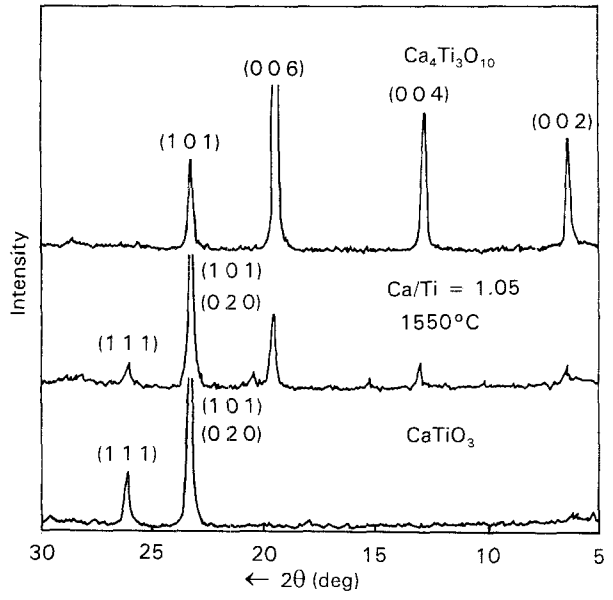

Figure 2 A comparison of partial X-ray diffractograms for $CaTiO_3$, the sample with Ca/Ti ratio of 1.05, and $Ca_4Ti_3O_{10}$.

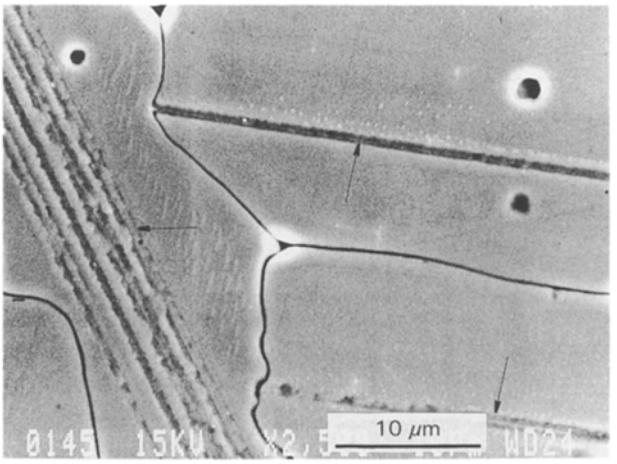

Figure 3 Scanning electron micrograph of the sample with a Ca/Ti ratio of 1.003, sintered for 1 h at 1550 °C. The marked lamellar phase is $Ca_4Ti_3O_{10}$.

the XRD results this phase was identified as $Ca_4Ti_3O_{10}$. The microstructures of polished and thermally etched samples with Ca/Ti ratios of 1.000, 1.003, 1.005, 1.01, 1.02, 1.05 and 1.1 are shown in Fig. 4. The lamellar phase ($Ca_4Ti_3O_{10}$) is clearly visible in the microstructure of all the samples, with the exception of the stoichiometric composition with Ca/Ti = 1.00. The amount of $Ca_4Ti_3O_{10}$ increases with increasing Ca/Ti ratio. Its appearance promotes the anisotropic growth of $CaTiO_3$ grains.

Since XRD failed to detect $Ca_4Ti_3O_{10}$ in samples with a Ca/Ti ratio < 1.05, which was probably due to the low content of this phase in the sample, the composition of the lamellar phase for samples with a Ca/Ti ratio < 1.05 was determined by WDS. A typical point scan result across the lamellar phase in the sample with a Ca/Ti ratio of 1.005 is shown in Fig. 5. Quantitative results were determined using the standard ZAF correction procedure (Z-atomic number, A-absorption and F-fluorescence). The precision of the analysis was estimated to be ± 2%. The maximum value for calcium concentration in the middle of the lamella is 23.2 ± 0.5 at %. This value is comparable with the calculated theoretical value for the calcium content in $Ca_4Ti_3O_{10}$, which is 23.53 at %. A slightly lower value for the measured calcium concentration is expected due to the morphology of the $Ca_4Ti_3O_{10}$ phase. Namely, the lamellae of $Ca_4Ti_3O_{10}$ are very thin, suggesting that some of the detected X-rays were also generated from the matrix ($CaTiO_3$), which has a lower calcium content than $Ca_4Ti_3O_{10}$.

Transmission electron microscopy (TEM) observations were not undertaken as a careful phase study. Nevertheless, important evidence regarding the mode of CaO incorporation in $CaTiO_3$ was revealed. TEM of selected samples sintered at 1350 °C showed that a fair proportion of $CaTiO_3$ grains displayed disorder typical of intergrowth. Fig. 6, which represents the lattice image of a $CaTiO_3$ thin foil, shows the presence of planar faults which are parallel to the (1 0 1) lattice planes of $CaTiO_3$. Such planar faults were never observed in stoichiometric $CaTiO_3$, but only in samples with a ratio of Ca/Ti > 1. The planar faults in Fig. 6 were not analysed in detail, but if the assumption is

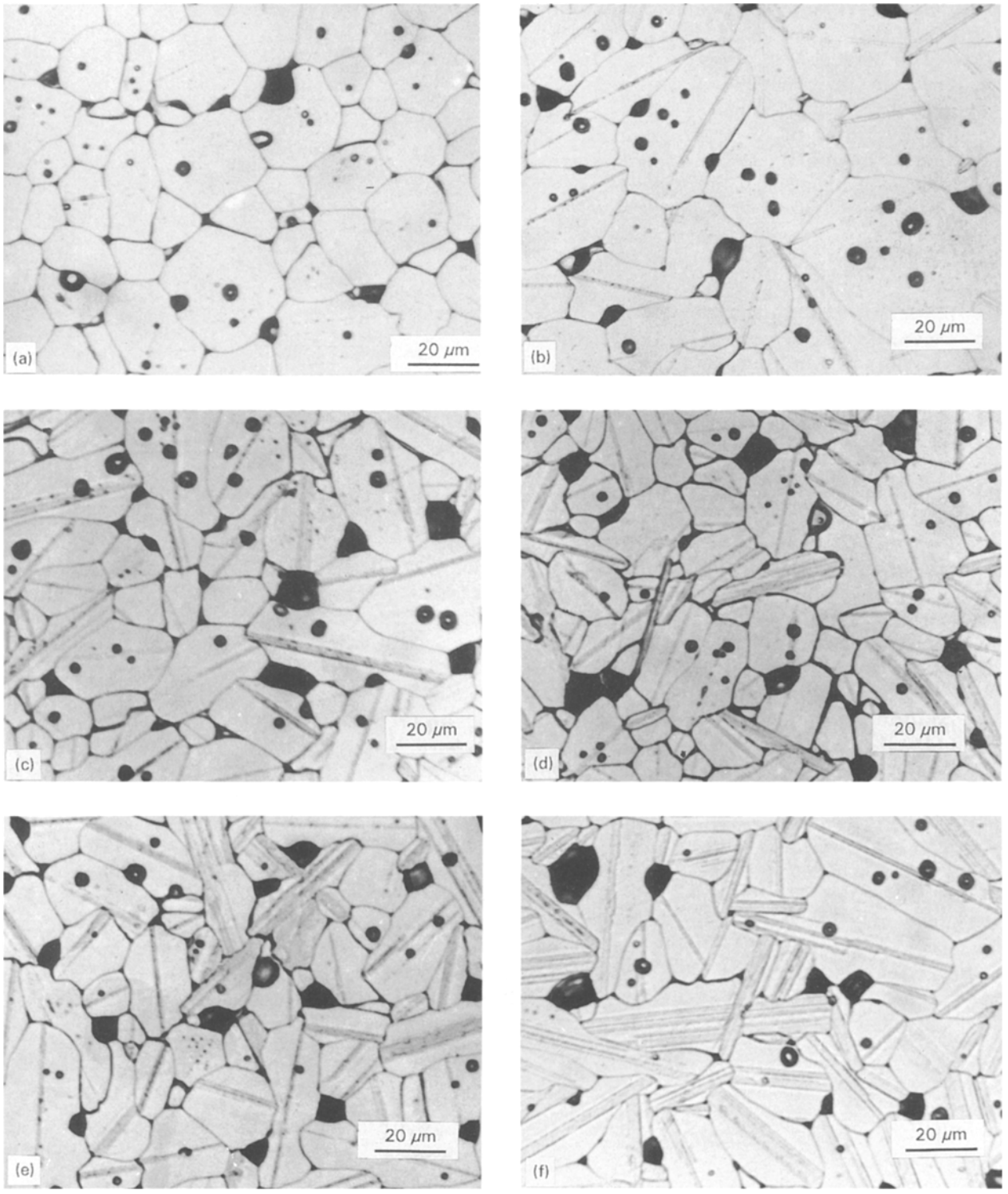

Figure 4 Optical micrographs of thermally etched samples with different Ca/Ti ratios: (a) 1.00, (b) 1.003, (c) 1.005, (d) 1.01, (e) 1.02, (f) 1.05, (g) 1.1 at $T = 1550\,^{\circ}C$, 24 h (magnification $\times 368$).

made that they have the same structure as occurs between the perovskite lamellae in $Ca_4Ti_3O_{10}$ and $Ca_3Ti_2O_7$ [5], they can be regarded as layers of CaO which are coherently intergrown with $CaTiO_3$ (Ruddlesden–Popper type faults). In this case the crystal should have an overall composition slightly richer in CaO than stoichiometric $CaTiO_3$. By ordering of CaO layers, various homologous oxides $Ca_{n+1}Ti_nO_{3n+1}$ can be formed, as seen in Fig. 6, where lamellae of the oxides $Ca_6Ti_5O_{16}$, $Ca_8Ti_7O_{22}$ and $Ca_9Ti_8O_{25}$ are coherently intergrown with $CaTiO_3$.

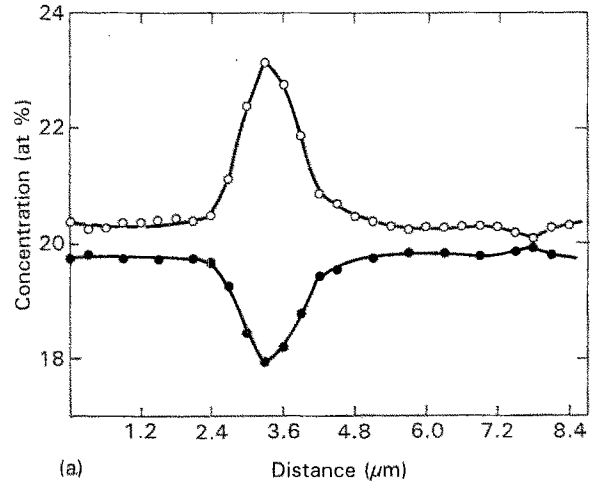

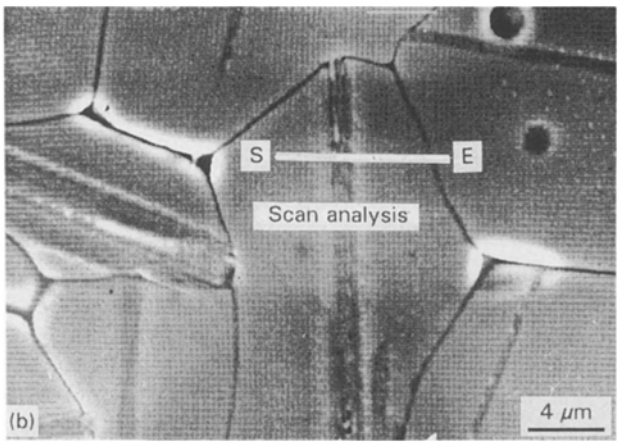

Figure 5 Results of quantitative step scan WDS microanalysis of the lamellar phase in the sample with Ca/Ti ratio of 1.005 (a): (○) at % Ca, (●) at % Ti. The beam path during the analysis is marked on the scanning electron micrograph (b): (S) start, (E) end.

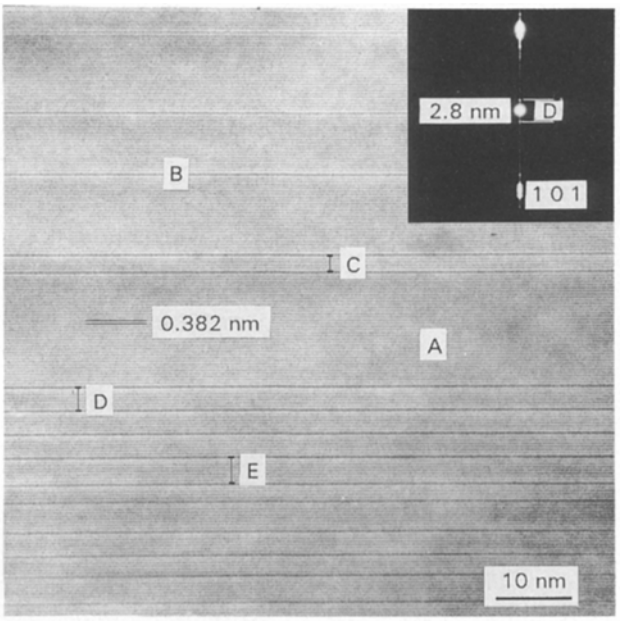

Figure 6 Lattice image of $CaTiO_3$ doped with 2 mol % CaO showing (1 0 1) lattice fringes of $CaTiO_3$. $CaTiO_3$ crystal (A) contains isolated planar faults (B) and intergrown lamellae of the oxides $Ca_6Ti_5O_{16}$ (C), $Ca_8Ti_7O_{22}$ (D) and $Ca_9Ti_8O_{25}$ (E). $T = 1350\,°C$, 4 h.

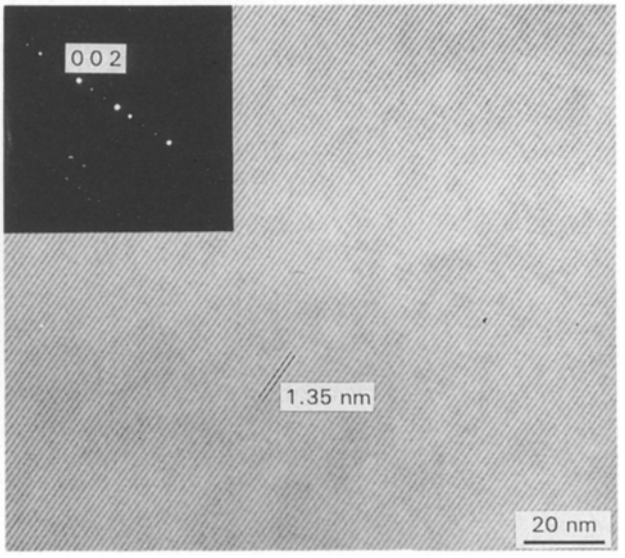

Figure 7 (0 0 2) lattice fringes of well ordered $Ca_4Ti_3O_{10}$ crystal in the sample with a Ca/Ti ratio of 1.02, sintered for 4 h at 1550 °C.

The weak electron diffraction of approximately 2.8 nm (marked D) belongs to the (0 0 1) lattice distance of a few ordered $Ca_8Ti_7O_{22}$ slabs. It should be mentioned that a distinct difference existed between the samples with $Ca/Ti > 1$ that were sintered at 1350 °C and those sintered at 1550 °C. In the samples sintered at 1550 °C, no isolated or partly ordered planar faults were detected, but only areas of well ordered slabs of the compound $Ca_4Ti_3O_{10}$ (Fig. 7) which were coherently intergrown with $CaTiO_3$. It was concluded that any excess CaO in $CaTiO_3$ will cause the formation of Ruddlesden–Popper type planar faults, which are in fact layers of CaO interleaved with perovskite layers. At lower temperature (1350 °C), these planar faults are isolated, or partly ordered. Eventually, at higher temperatures, when the diffusional processes are faster, these planar faults tend to form slabs of thermodynamically stable $Ca_4Ti_3O_{10}$ compounds, which are coherently intergrown with the $CaTiO_3$ matrix. A detailed TEM study of the nature of the planar faults and the coherent intergrowth between different compounds in the $CaTiO_3$–CaO system is currently in progress and will be published elsewhere.

The electrical conductivities measured as a function of oxygen partial pressure in $CaTiO_3$ with $Ca/Ti = 1.00$ and 1.02 at 800 °C are given in Fig. 8. In both cases, the electrical conductivity changed from *p*- to *n*-type as the oxygen partial pressure was decreased. No significant shift in the conductivity profile was noticed that could be attributed to an increase of $V_O^{\cdot\cdot}$ due to the solubility of excess CaO in $CaTiO_3$ according to Equations 1 and 3. Since changes in $V_O^{\cdot\cdot}$ of the order of 100 p.p.m. can be detected by measuring the equilibrium electrical conductivity, it was concluded that the solubility of excess CaO in $CaTiO_3$ is < 100 p.p.m., and is insufficient to modify the defect concentration relative to the natural impurity content. In principle, excess CaO could be incorporated in $CaTiO_3$ according to Equations 1 and 3 without the creation of free $V_O^{\cdot\cdot}$ if the point defects $V_O^{\cdot\cdot}$, $V_{Ti}^{''''}$ and Ca_{Ti}'' were associated into defect complexes. However, the observation of $V_O^{\cdot\cdot}$ as a shift in conductivity profile

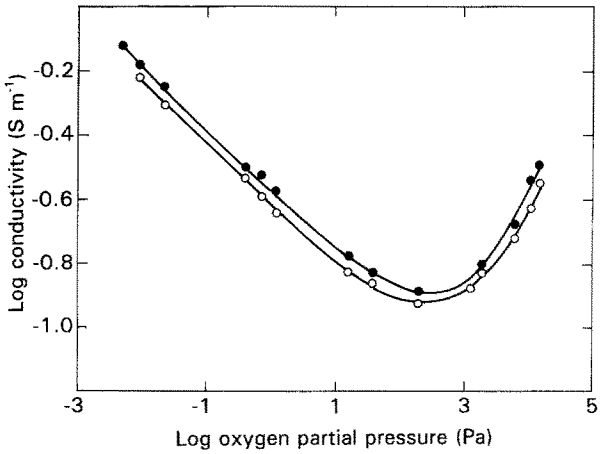

Figure 8 Equilibrium electrical conductivity at 800 °C for stoichiometric and CaO–excess $CaTiO_3$: (●) Ca/Ti = 1.00, (○) Ca/Ti = 1.02.

in acceptor-doped $BaTiO_3$ [26] indicates that complex formation at high temperatures is not important in these perovskites with high dielectric constant. Also, cation vacancies have long been recognized as unfavourable defects in acceptor doped alkaline-earth perovskites. Similarly, calculations to establish the energetic preference of Ca to substitute on Ti sites in $CaTiO_3$ by Udayakumar and Cormack [25] showed that substitution of Ca^{+2} ions on Ti sites as Ca''_{Ti} is not likely to occur. The measured low solubility of CaO in $CaTiO_3$ agrees with the fact that the incorporation of excess CaO does not occur by point defect formation.

4. Conclusions

The solubility of CaO in $CaTiO_3$ was determined to be no more than 100 p.p.m. A second phase, $Ca_4Ti_3O_{10}$, was observed for samples having > 0.3 mol % excess CaO (Ca/Ti > 1.003) by direct microscopic observations. The incorporation of excess CaO in $CaTiO_3$ results in formation of randomly distributed Ruddlesden–Popper type planar faults which are parallel to the (1 0 1) lattice planes of $CaTiO_3$. Their concentration probably depends on the initial local stoichiometries encountered in the preparation. These planar faults, which are in fact layers of CaO, can form various homologous oxides of $Ca_{n+1}Ti_nO_{3n+1}$ type but only as intermediate phases. When chemical equilibrium is reached, the stable compound $Ca_4Ti_3O_{10}$ is formed, which is coherently intergrown with $CaTiO_3$.

Acknowledgements

The authors express their thanks to Dr Janez Holc for helpful suggestions and assistance in measurement of electrical conductivity. The financial support of the Ministry of Science and Technology of the Republic of Slovenia is gratefully acknowledged.

References

1. H. van WARTENBERG, H. J. REUSCH and E. SARAN, *Z. Anorg. Chem.* **230** (1937) 257.
2. S. UMEZU and F. KAKIUCHI, *Nippon Kogyo Kwaisi* **46** (1930) 866.
3. M. FUKUSHIMA, *Kinzoku no Kenkyu* **11** (1934) 590.
4. R. C. DeVRIES, R. ROY and E. F. OSBORN, *J. Phys. Chem.* **58** (1954) 1069.
5. R. S. ROTH, *J. Res. Natl. Bur. Std.* **61** (1958) 437.
6. W. KWESTROO and H. A. M. PAPPING, *J. Amer. Ceram. Soc.* **42** (1959) 292.
7. A. COCCO, *Rend. Seminar Fac. Sci. Univ. Cagliari* **25** (1955) 164.
8. A. JONGEJAN and A. L. WILKINS, *J. Less-Common Metals* **20** (1970) 273.
9. F. A. KRÖGER and H. J. VINK in "Solid State Physics", Vol. 3, edited by F. Seitz and D. Turnbull (Academic Press, New York, 1956) p. 307.
10. G. V. LEWIS and C. R. A. CATLOW, *J. Phys. Chem. Solids* **47** (1986) 89.
11. N. G. EROR and D. M. SMYTH, *J. Solid State Chem.* **24** (1978) 235.
12. J. DANIELS, K. H. HARDTL, D. HENNINGS and R. WERNICKE, *Philips Res. Rep.* **31** (1976) 487.
13. Y. H. HAN, J. B. APPLEBY and D. M. SMYTH, *J. Amer. Ceram. Soc.* **70** (1987) 96.
14. H. M. CHAN, M. P. HARMER, M. LAL and D. M. SMYTH in "Proceedings of Materials Research Society Symposium", Vol. 31, edited by W. Krakow, D. A. Smith and L. W. Hobbs (Elsevier, New York, 1984) p. 345.
15. S. N. RUDDLESDEN and P. POPPER, *Acta Cryst.* **10** (1957) 538.
16. *Idem, ibid.* **11** (1958) 54.
17. K. R. UDAYAKUMAR and A. N. CORMACK, *J. Amer. Ceram. Soc.* **71** (1988) C-496.
18. R. J. D. TILLEY, *J. Solid State Chem.* **21** (1977) 293.
19. M. FUJIMOTO, J. TANAKA and S. SHIRASAKI, *Jpn J. Appl. Phys.* **27** (1988) 1162.
20. U. BALACHANDRAN and N. G. EROR, *Mater. Sci. Engng* **54** (1982) 221.
21. U. BALACHANDRAN, B. ODEKIRK and N. G. EROR, *J. Solid State Chem.* **41** (1982) 185.
22. Y. H. HAN, M. P. HARMER, Y. H. HU and D. M. Smyth in "Transport in Nonstoichiometric Compounds", edited by G. Simkovich and V. S. Stubican (Plenum Press, New York, 1985) p. 73.
23. C. N. BERGLUND and W. S. BAER, *Phys. Rev.* **157** (1967) 358.
24. X. W. ZHANG, Y. H. HAN, M. LAL and D. M. SMYTH, *J. Amer. Ceram. Soc.* **70** (1987) 100.
25. K. R. UDAYAKUMAR and A. N. CORMACK, *J. Phys. Chem. Solids* **50** (1989) 55.
26. N. H. CHAN, R. K. SHARMA and D. M. SMYTH, *J. Amer. Ceram. Soc.* **65** (1982) 167.

Received 25 March 1993
and accepted 16 May 1994